Strong TCR Conservation and Altered T Cell Cross-Reactivity Characterize a B*57-Restricted Immune Response in HIV-1 Infection

Geraldine M. A. Gillespie, Guillaume Stewart-Jones, Jaya Rengasamy, Tara Beattie, Job. J. Bwayo, Francis A. Plummer, Rupert Kaul, Andrew J. McMichael, Philippa Easterbrook, Tao Dong, E. Yvonne Jones and Sarah L. Rowland-Jones

J Immunol 2006; 177:3893-3902; ;
http://www.jimmunol.org/content/177/6/3893

The Journal of Immunology is published twice each month by
The American Association of Immunologists, Inc.,
9650 Rockville Pike, Bethesda, MD 20814-3994.

Print ISSN: 0022-1767 Online ISSN: 1550-6606.

Strong TCR Conservation and Altered T Cell Cross-Reactivity Characterize a B*57-Restricted Immune Response in HIV-1 Infection[1,2]

Geraldine M. A. Gillespie,[3,4]* Guillaume Stewart-Jones,[4†] Jaya Rengasamy,* Tara Beattie,* Job. J. Bwayo,[‡] Francis A. Plummer,[§] Rupert Kaul,[¶] Andrew J. McMichael,* Philippa Easterbrook,[‖] Tao Dong,* E. Yvonne Jones,[†] and Sarah L. Rowland-Jones*

HLA-B*57 is associated with slower disease progression to AIDS, and CD8$^+$ T cell responses to B*57-restricted epitopes are thought to contribute to this protective effect. In this study, we evaluate the B*57-restricted p24 KAFSPEVIPMF (KF11) immune response which is immunodominant during chronic infection. Previously, we observed that the KF11 clade variants KGFNPEVIPMF [A2G,S4N] and KAFNPEIIMPF [S4N,V7I], sharing a position 4 mutation, are differentially recognized by KF11-specific T cells. By combining structural and cellular studies, we now demonstrate that the KF11 and [A2G,S4N] epitopes induce distinct functional responses in [A2G,S4N] and KF11-specific T cells, respectively, despite minimal structural differences between the individual B*57-peptide complexes. Recently, we also elucidated the highly distinct structure of KF11 in complex with B*5703, and have now characterized the CD8$^+$ T cell repertoire recognizing this epitope. We now report striking features of TCR conservation both in terms of TCR Vα and Vβ chain usage, and throughout the hypervariable region. Collectively, our findings highlight unusual features of the B*5701/B*5703-KF11-specific immune responses which could influence disease progression and that might be important to consider when designing future vaccine regimens. *The Journal of Immunology,* **2006, 177: 3893–3902.**

The MHC class I genes represent crucial host factors influencing disease outcome during HIV-1 infection. MHC class I molecules dictate the repertoire of epitopes presented to CD8$^+$ T cell and, therefore, the nature of the immune response against HIV. Maximum heterozygosity at the MHC class I loci is favorable, and individual MHC class I alleles also associate with prolonged AIDS-free survival, of which B*27 and B*57 are consistently described (1).

The influence of the MHC class I loci on clinical outcome warrants further investigation to further our understanding of disease pathogenesis and to direct the generation of effective vaccines. The heterozygous advantage at the MHC class I locus probably reflects the availability of distinct MHC class I molecules to present diverse epitopes to T lymphocytes, resulting in broader immune responses, and delaying the incidence of viral immune evasion. The preference for individual MHC class I alleles might reflect their ability to present conserved viral epitopes to CD8$^+$ T cells; the conservation of a single immunodominant epitope, namely the *gag*-derived KRWIILGLNK (KK10) peptide, appears to account for the association of B*27 with prolonged AIDS-free survival in infection. KK10 requires a series of complex mutations, both internal and external to the epitope, to enable the emergence of a successfully mutated epitope that evades immune recognition with eventual onset of AIDS (2). The HLA class I subtype B*57 is consistently associated with slower disease progression in HIV-1 infection, particularly the *B*5701* and *B*5703* alleles which relate to better clinical outcome in Caucasian and African patients, respectively (3–6). The mechanism(s) by which B*57 confers favorable outcome are not fully understood. In contrast to B*27, a large number of potent B*5701/03-restricted HIV-1 epitopes have been described, most notably the *gag* epitopes ISPRTLNAW (IW9), TSTLQEQIGW (TW10), and KAFSPEVIPMF (KF11), which are immunodominant, and map to the p24 capsid protein (7) (5, 8). Previously, it was assumed these p24-derived epitopes were highly conserved, however, the loss of B*57 epitope recognition through escape mutation has recently been described. First, a single point mutation arising in the TW10 epitope (T242N) during the acute phase of HIV-1 infection results in escape from CD8$^+$ T cell recognition (9). Second, an epitope-flanking mutation adjacent to the IW9 epitope (A to P mutation) abrogates processing of the IW9 epitope in B and C clade infections. Although not associated with an increase in viral load, it has been suggested that the TW10 mutation impacts on viral fitness as it is lost upon transmission to B*57-negative individuals. The IW9 flanking mutation is associated with a 20-fold increase in viral load, although it is unclear whether this mutation precipitates clinical progression.

* Medical Research Council Human Immunology Unit, Weatherall Institute of Molecular Medicine, John Radcliffe Hospital, Headington, Oxford, United Kingdom; [†]Division of Structural Biology, Wellcome Trust Centre for Human Genetics, Roosevelt Drive, Oxford, United Kingdom; [‡]Department of Medical Microbiology, University of Nairobi, Nairobi, Kenya; [§]Department of Medical Microbiology, University of Manitoba, Winnipeg, Manitoba, Canada; [¶]Division of Infectious Diseases, Department of Medicine, University of Toronto, Toronto, Ontario, Canada; and [‖]Academic Department of HIV/GUM, Guy's, King's, and St. Thomas' School of Medicine, Weston Education Centre, London, United Kingdom

Received for publication March 30, 2006. Accepted for publication June 16, 2006.

The costs of publication of this article were defrayed in part by the payment of page charges. This article must therefore be hereby marked *advertisement* in accordance with 18 U.S.C. Section 1734 solely to indicate this fact.

[1] This work was supported by Elizabeth Glaser Pediatric AIDS Foundation Grant No. 77474-28-PF, and funding from the Medical Research Council, Wellcome Trust, and Cancer Research U.K.

[2] Atomic coordinates and structure factor amplitudes for the HLA-B*5703-A2G,S4N and the HLA-B*5703-S4N,V7I complexes have been deposited in the Protein Data Bank under accession codes 2HJK and 2HJL, respectively.

[3] Address correspondence and reprint requests to Dr. Geraldine M. A. Gillespie, Medical Research Council Human Immunology Unit, Weatherall Institute of Molecular Medicine, John Radcliffe Hospital, Headington, Oxford, OX3 9DS, U.K. E-mail address: ggillesp@hammer.imm.ox.ac.uk

[4] G.M.A.G. and G.S.-J. contributed equally to this study.

0022-1767/06/$02.00

The focus of our study is the B*5701/03-restricted KF11 immune response which prevails during chronic HIV-1 infection (10, 11). Importantly, we now show this to be the immunodominant B*57-restricted response in a cross-sectional study of chronically infected B*5701$^+$ slow progressors harboring both TW10- and IW9-mutated viruses.

KF11 is also interesting from a structural perspective. We have recently solved the crystal structure of B*5703 in complex with the KF11 epitope (12). KF11 adopts a distinctive conformation that differs significantly from previously published human peptide-MHC class I complexes. The central region of the epitope encompassing the position (p) 5 to p9 amino acids buckles high above the peptide-binding groove. Proline residues at p5 and p9 form the corner stones of the "bulge" structure, and stabilize the hairpin-like conformation. Together with peptide residues F3 and I8, they form a network of hydrophobic contacts at the core of the central bulge structure. As epitope residues E6 and V7 are located at the crest of the bulge, their side chains are solvent-exposed and accessible to responding TCRs.

Although KF11 is highly conserved in B clade viruses, diverse KF11 clade variants are documented in the Los Alamos Database. Previously, we assessed cross-reactivity to these variants, and observed broad but differential recognition of the epitopes (10). Interestingly, much of our functional data are readily explained by our structure analysis; mutations involving the p5 proline (P to Q mutation, (P5Q)) and the p3 phenylalanine (F to L mutation, (F3L)), for example, resulted in diminished T cell recognition, most likely due to destabilization of the central bulge structure. However, the common clade variant KGFNPEVIPMF ([A2G,S4N]), produced an inconsistent pattern of cross-recognition, a result open to interpretation in terms of our B*5703-KF11 structural analysis. Although KF11 represents the dominant A and B clade virus sequence, [A2G,S4N] is categorized as A/C clade virus and is the second most common variant in the database, where it accounts for 7% KF11 clade variant sequence entries (April 2006). To date, the [A2G,S4N] variant has only been isolated from B*5703$^+$ donors, and it is not clear whether this epitope originally emerged as an escape variant of KF11.

If the KF11 immune response is also associated with better immune control, it is important that we also consider the immune response to [A2G,S4N] particularly given the association of B*5703 with slow disease progression, and the prevalence of this viral clade in African cohorts. Determining the degree of KF11 and [A2G,S4N] cross-reactivity in B*5703$^+$ patients is also important to evaluate, particularly from the perspective of vaccine development. Consequently, in this study, we investigate the recognition of KF11 and [A2G,S4N] using a number of strategies. First, we performed functional studies of KF11 and [A2G,S4N] to determine whether CD8$^+$ T cell recognition patterns vary according to the prevailing virus sequence in B*5701$^+$ and B*5703$^+$ patients. Second, we performed structural studies to ascertain whether the peptide variants adopt different conformations when in complex with HLA-B*5703 and are differentially presented to CD8$^+$ T lymphocytes. Finally, we assessed TCR usage and CDR3 loop sequence analysis to determine whether recognition of these epitopes is a function of similar or distinct TCR clonotypes.

Materials and Methods

Subjects

Eleven B*57$^+$ subjects were enrolled in this study (Table I). Ethical approval was obtained from the relevant ethical committees, and all patients gave consent to donate blood. HLA class I typing was performed by the amplification refractory mutation systems PCR using sequence specific primers.

Isolation of PBMCs

PBMCs were isolated from heparinized venous blood by Ficoll-Hypaque (Nycomed) density gradient centrifugation. Cells were maintained in RPMI 1640 (Sigma-Aldrich) supplemented with 10% human serum 100 IU of penicillin/L, 100 mg of streptomycin/L (Invitrogen Life Technologies), referred to herein as H10.

Peptide synthesis

B*57-restricted peptides were synthesized by F-moc chemistry using a Zinnser analytical synthesizer (Advanced Chemtech) and purity was determined by HPLC (Table II).

Generation of MHC class I tetramers

The generation of HLA-B*57 tetramers was performed according to previously described protocols (13, 14). Avidin-PE (Sigma-Aldrich) and streptavidin allophycocyanin (BD Biosciences) were used as fluorochromes.

Establishment of CTL lines

A total of 5×10^6 PBMCs were incubated with 50 μM peptide at 37°C for 1 h, before resuspension in H10 supplemented with 25 ng/ml IL-7. Cells were fed on day 3 with rIL-2 at a concentration of 100 U/ml (10, 15).

Generation of CD8$^+$ T cell clones.

Tetramer staining and magnetic (MACS; Miltenyi Biotec) bead selection was used to generate CD8$^+$ T cell clones. A total of 1×10^6 cells (day 14 CTL line) were stained with B*57-PE-conjugated tetramers and 20 μl of anti-PE microbeads before purification using MS$^+$/MR$^+$ MACS columns (10). Purified cells were cloned at frequencies of 1, 2, and 3 cells/well into

Table I. *Demographics of B*57$^+$ long-term nonprogressor patients*

Patient[a]	Ethnicity	Year of Seroconversion (s)/ Diagnosis (d)	Viral Load (copies/mL)	CD4 Count (cells/μl)	Current Status	HLA-B*57	Dominant Virus
LON005	Caucasian	1986 (s)	295,001	420	np	B*5701	KAFSPEVIPMF
LON065	Caucasian	1984 (s)	60,900	1,921	np	B*5701	KAFSPEVIPMF
LON113	Caucasian	1984 (s)	<50	414	np	B*5701	KAFSPEVIPMF
LON140	Black Carribean	1985 (s)	46,400	234	sp	B*5701	KAFSPEVIPMF
LON201	Caucasian	1988 (s)	192	720	np	B*5701	KAFSPEVIPMF
LON202	Caucasian	1989 (s)	<50	1063	np	B*5701	KAFSPEVIPMF
LON208	Caucasian	1992 (s)	<50	898	np	B*5701	KGFSPEVIPMF
OX AG	Caucasian	1999 (d)	10^6	10		B*5701	KAFSPEVIPMF
OX MS	Caucasian	1997 (d)	37,600	590		B*5701	KAFSPEVIPMF
ML005	Black African		390	ND	p	B*5703	KGFNPEVIPMF
ML525	Black African		820	ND	p	B*5703	KGFNPEVIPMF[b]

[a] LON denotes patients from the Kings College Cohort, London; OX denotes patients from the John Warin Ward, Oxford; and ML represents patients from the Kenyan Cohort. Current status abbreviations are as follows: Sp, slow progressor, np, non-progressor, and p, progressor. The clinical status of OX AG and OX MS are currently unknown.
[b] The KAFSPEVIPMF epitope was also identified in patient ML525 and represented ~25% of the viral sequences analyzed ($n = 24$).

Table II. *HLA*B57 epitopes*

Protein	Sequence Location	Epitope	Abbreviation
Previously defined B*57-restricted epitopes			
GAG p24	aa 15–23	ISPRTLNAW	IW9
	aa 30–40	KAFSPEVIPMF	KF11
	aa 30–37	KAFSPEVI	KI8
	aa 108–118	TSTLQEQIGW	TW10
	aa 176–184	QASQEVKNW	QW10
Integrase	aa 173–181	KTAVQMAVF	intKF9
Rev	aa 14–23	KAVRLIKFLY	revKY10
Nef	aa 116–125	HTQGYFPDWQ	nefHQ10
	aa 120–128	YFPDWQNYT	nefYT9
Vpr	aa 30–38	AVRHFPRIW	vprAV9
Vif	aa 31–39	ISKKAKGWF	vif IF9
RT	aa 244–252	IVLPEKDSW	rtIW9
		KITTESIVIW	rtKW9
KF11 p4 variants (cellular assays)			
		KAFSPEVIPMF	KF11
		K**G**F**N**PEVIPMF	[A2G,S4N]
		KAF**A**PEVIPMF	p4A
		KAF**D**PEVIPMF	p4D
		KAF**I**PEVIPMF	p4I
		KAF**Q**PEVIPMF	p4Q
		KAF**T**PEVIPMF	p4T
		KAF**N**PE**I**IPMF	[S4N,V7I]
KF11 clade variants (structural studies)			
		K**G**F**N**PEVIPMF	[A2G,S4N]
		KAF**N**PE**I**IPMF	[S2N,V7I]

[a] KF11 amino acid changes at positions 2, 4 and 7 are highlighted in boldface type.

U-bottom 96-well places containing 1.5×10^4 peptide-pulsed irradiated autologous B cells (BCL),[5] 1×10^5 irradiated mixed allogeneic PBMCs, and a 20 μg/ml PHA. Clones were supplemented with 100 IU/ml rIl-2 on day 3. Specificity was assessed by tetramer staining after 2 wk.

Peptide-based IFN-γ ELISPOT assay

A standard ELISPOT assay was used to detect IFN-γ release by PBMCs (16). Responses are reported as spot-forming units (SFUs) per million PBMCs. SFUs double that observed with medium alone, and in excess of 20 per million PBMCs, were considered positive.

Intracellular cytokine staining.

A total of 200,000 T cell clones was incubated with 100,000 BCLs either pulsed with 10 μM peptide or medium alone at 37°C. A total of 10 μg/ml brefeldin A (Sigma-Aldrich) was added during the second hour of incubation. After 6 h, cells were washed in BD Perm/Wash buffer before fixation/permeabilization in Cytofix/Cytoperm buffer (BD Biosciences). Staining was performed for 30 min on ice using the following panel of mAbs: anti-human (h) IFN-γ FITC, anti-hTNF-α PE (Dako), and anti-hCD8 PerCP (BD Biosciences). Cells were washed and stored in PBS-5% formaldehyde (17).

CD107a and CD107b expression

A total of 200,000 T cell clones was incubated either 100,000 autologous BCLs pulsed with 10 μM peptide or with medium alone, plus 5 μl of both CD107a- and CD107b-FITC-labeled mAbs at 37°C (BD Biosciences). Golgi-Stop (BD Biosciences) was added to each sample after the first hour of incubation (18). Following 6 h, cells stained with anti-hCD8 PerCP (BD Biosciences) and fixed in 5% formaldehyde-PBS before analysis.

Tetramer decay analysis

To test whether B*57^{KF11} and B*57^{A2G,S4N} tetramers bound [A2G,S4N]-specific T cell clones with similar affinities, a tetramer decay analysis was performed (19). A total of 2×10^6 T cells from clone ML525 p5–10 was incubated with B*5703^{KF11} and B*5703^{A2G,S4N} PE tetramers at 4°C for 45 min.

Following extensive washing in PBA-0.1% BSA, cells were resuspended and aliquot $t = 0$ was removed. A 5-fold excess of allophycocyanin-conjugated B*5703^{A2G,S4N} tetramer was added to each tube, and samples were incubated on ice. At 20-min intervals, aliquots corresponding to $t = 1$, $t = 2$, etc., were removed, washed, and fixed in PBS-5% formaldehyde. Tetramer binding was analyzed by flow cytometry, and the natural log of the mean geometric intensity of FL-2 immunofluorescence for each samples were plotted against sampling time.

Sequencing of p24 epitopes

gDNA (proviral DNA) was isolated from PBMCs using the PureGene DNA Isolation kit (Gentra Systems) from which p24 was amplified by seminested PCR (10). The p24 5′ and 3′ outer primers include primer-GAGATA(A/C)(A/G)AGACACCAA(A/G)GAAGC and CATGCTGTC ATCATTTCTTCTA were used during the first round of PCR amplifications, and 5′ primer CAGCCAAAATTACCCTATAGTGC plus 3′ outer from the first-round amplifications were used during second-round PCRs. Nested p24 PCR products were cloned into TOPO TA vectors (Invitrogen Life Technologies). Ampicillin-resistant (Amp^R) colonies were expanded and plasmid DNA was isolated for sequence analysis.

Staining of tetramer-reactive T cells with V region-specific TCR mAbs

Staining of B*57-reactive T cells using V region-specific mAbs and tetramer was performed as described previously (20). A total of 5×10^5 fresh PBMCs or 5×10^4 CTL lines were stained with a panel of TCR-specific Abs and rabbit anti-mouse Ab conjugated to FITC before labeling with B*57 tetramers and anti-CD8 PerCP (BD Biosciences). Cells were fixed in PBS-5% formaldehyde solution.

Sequencing of TCR Vα and Vβ segments

mRNA was isolated from 1×10^6 CD8$^+$ T cell clones using TriReagent (Sigma-Aldrich) and cDNA was synthesized using the cDNA Cycle kit for RT-PCR (Invitrogen Life Technologies). A panel of Vβ- and Vα-specific primers were used to screen for TCR usage by PCR analysis (21). PCR

[5] Abbreviations used in this paper: BCL, autologous B cell; SFU, spot-forming unit; h, human; ICS, intracellular cytokine staining; FSC, forward scatter; SSC, side scatter.

amplification was conducted using Red *Taq* Ready Mix PCR Mix (Sigma-Aldrich). Control reactions included V region primers and H_2O. TCR PCR products were cloned by TOPO TA cloning (Invitrogen Reaction), and plasmid DNA was isolated for sequencing analysis.

Protein crystallization and data collection

Crystallizations were done by the sitting drop vapor diffusion technique. After equilibration, and cross-seeding from wild-type HLA-B*5703-KF11 crystals, single crystals of HLA-B*5703-peptide complexes were obtained from a reservoir condition of 16% Peg 8000, 50 mM MES (pH 6.5). The largest crystals were soaked briefly and sequentially in mother liquor solutions supplemented with 10% and 20% glycerol, then flash-cooled and maintained at 100 K in a cryostream (Oxford Cryosystems). The HLA B*5703-KGFNPEVIPMF [A2G,S4N] and HLA B*5703-KAFNPEIIPMF [S4N,V7I] data sets were collected at station ID14 EH1 of the European Synchrotron Radiation Facility (ESRF) (Grenoble, France) with an ADSC-Q4 (Area Detector Systems) CCD detector. Both B*5703-peptide complexes belonged to the orthorhombic space group $P2_12_12_1$. Diffraction data were autoindexed with the program DENZO and scaled with the program SCALEPACK (22). Statistics are summarized in Table III.

Structure determination and analysis

Crystal structures were determined by molecular replacement using the program EPMR (23). The H chain and β2m domains from the HLA B*5703-KF11 structure (12) were used as the search probe (peptide and bound water coordinates omitted). This model yielded unambiguous solutions for both variant B*5703-peptide complexes with correlation coefficients of ~0.7 and *R* factors of ~35% for data between 30 and 4Å. Using CNS (24), the models were subjected to several rounds of rigid body refinement of individual domains (a1/a2, a3, β2m) after which *Fo* − *Fc* difference maps calculated for both complexes revealed the presence of the 11-mer peptides when displayed in the graphics program O (25).

The peptides were modeled into the *Fo* − *Fc* difference density maps and further rounds of refinement were conducted using standard CNS protocols for bulk solvent correction and overall anisotropic *B*-factor scaling, positional refinement, simulated annealing and individual *B*-factor refinement. Manual refitting of the models was conducted using O. Conjugate gradient minimization refinement was performed at the final stages of crystallographic refinements after water picking with ARPw/ARP (26), using a restrained refinement algorithm in REFMAC5 (27). Structural superpositions were conducted using program SHP (28) and the figures were generated in Bobscript (29)

Results

*B*57-specific CD8$^+$ T cell responses in B*5701$^+$ patients.*

First, we assessed which of the previously mapped B*57 epitopes were immunodominant during chronic HIV-1 infection. We used the standard ELISPOT assay to evaluate IFN-γ secretion in response to B*57-restricted epitopes including *gag*, *nef*, *integrase*, *rev*, *vpr*, *vpu*, and *vif* (Table II, "Previously defined B*57-restricted epitopes" section) in 9 of the 11 patients. Our results demonstrate that the p24 *gag* epitopes KAFSPEVIPMF (KF11) and ISPRTL NAW (IW9) were immunodominant both in terms of frequency and magnitude of recognition (Table IV).

Cellular analysis

Previously, we observed that the common A/C clade variant [A2G,S4N], and a second harboring a position 4 (p4) S to N mutation ([S4N,V7I]), were differentially recognized in B*5701$^+$ and B*5703$^+$ patients infected with the KF11 virus; in patients where [A2G,S4N] represented the dominant viral quasispecies, [A2G,S4N] and [S4N,V7I] were almost exclusively recognized with minimal recognition of other variants (10). Therefore, we questioned whether the amino acid change common to both variants, namely, the p4 residue, induced differential recognition. We generated KF11 variants with p4 mutations including A, D, I, Q, and T (Table II, "KF11 p4 variants" section), and used the standard ELISPOT assay to quantify IFN-γ secretion in response to the p4 variant epitopes in patients' PBMCs where either KF11 or [A2G,S4N] represented the dominant viral species. Our results demonstrate the differential recognition of the p4 KF11 variants, which varied according to the dominant viral sequence in individual patients (Fig. 1). In B*5703$^+$ donor ML005 where the predominant viral isolate represented the [A2G,S4N] variant, only the p4 D variant in addition to [A2G,S4N] generated strong responses. We observed similarly restricted recognition of p4 variants in B*5703$^+$ donor ML525 although we were unable to test the entire

Table III. *Crystallographic statistics*

	N4I7	G2N4
Data collection		
Space group	$P2_12_12_1$	$P2_12_12_1$
Unit cell		
Dimensions (Å) (a, b, c,)	50.4, 81.6, 109.1	50.5, 81.6, 109.8
Angles (°) (α,β,γ)	90, 90, 90	90, 90, 90
Source	ID14 EH1	ID14 EH1
Resolution (Å) (Highest resolution shell)	20-1.5 (1.55-1.50)	20-1.85 (1.92-1.85)
Measured reflections	1157669	761842
Unique reflections	574047	268724
Completeness (%)	99.1 (96.9)[b]	99.6 (99.4)[b]
I/σ (I)	24.3 (3.1)[b]	15.6 (3.1)[b]
R_{merge} (%)[a]	7.8 (70.6)[b]	11.4 (80.6)[b]
Refinement statistics		
Resolution range (Å)	20-1.5 (1.55-1.50)[b]	20-1.85 (1.92-1.85)[b]
R_{cryst}[c]	19.8	19.4
R_{free}[d]	22.6	23.7
Number of residues	384	384
Number of water molecules	774	543
Rms deviation from ideality		
Bond lengths (Å)	0.021	0.012
Bond angles (°)	1.681	1.40
Ramachandran Plot (%) (Favored, allowed, generous, disallowed)	(92.8, 6.6, 0.6, 0.0)	(93.7, 5.7, 0.6, 0.0)

[a] $R_{merge} = \Sigma_{hkl}II-<I>I/\Sigma_{hkl}I$ where I is the intensity of unique reflection hkl and <I> is the average over symmetry-related observations of unique reflection hkl.
[b] Numbers in parentheses correspond to the outermost shell of data.
[c] $R_{cryst} = \Sigma IF_{obs} - F_{calc}I/\Sigma F_{obs}$ where F_{obs} and F_{calc} are the observed and calculated structure factors, respectively.
[d] R_{free} is calculated as for R_{cryst} but using 5% of reflections sequestered before refinement.

Table IV. *The frequency and magnitude of B*57-restricted HIV-1 epitopes recognized in patients from the long-term nonprogressor King's College Cohort*[a]

B*57 Peptide Epitope	No. of Patients Who Recognized Epitope	Mean Response to Epitope (SFU/million PBMCs)
KI8	0	0
KF11	7	418
IW9	6	487
TW10	5	115
QW10	4	250
revKY10	3	46
nefYT9	4	131
nefHQ10	3	144
intKF9	6	109
vifIF9	4	106
vprAV9	4	89

[a] Peptide abbreviations are summarized in Table I; $n = 9$.

p4 panel due to sample limitation. These results are in sharp contrast to p4 variant recognition in B*5701$^+$ patients where KF11 represented the dominant virus: here D and N substitutions were poorly recognized whereas the p4 variants containing A, I, Q, T, and KF11 induced high levels of IFN-γ secretion.

We previously reported that at least in terms of tetramer binding and cytotoxicity, CD8$^+$ T cell clones from B*5701 and B*5703$^+$ KF11-infected patients were mostly cross-reactive for [A2G,S4N] (10). We extended this study to determine whether patients infected primarily with [A2G,S4N] viruses were also broadly cross-reactive for KF11. To date, the [A2G,S4N] variant has only been isolated from B*5703$^+$ donors; we identified two B*5703$^+$ patients in whom the [A2G,S4N] virus represented the dominant species, generated B*57 [A2G,S4N]-specific T cell clones from these patients and tested the ability of [A2G,S4N]-specific clones to produce IFN-γ and TNF-α in response to [A2G,S4N], KF11, and the p4 peptide variants by intracellular cytokine staining (ICS). Interestingly, all [A2G,S4N]-specific T cell clones preferentially produced cytokines in response to [A2G,S4N], with minimal responses induced by KF11 or the p4 variants (Fig. 2).

[A2G,S4N] represented the only viral sequence isolated from B*5703$^+$ donor ML005, whereas donor ML525 harbored both [A2G,S4N] and KF11 viruses at a frequency of 75 and 25% respectively. We questioned whether [A2G,S4N]-specific T cells and KF11-specific T cells from donor ML525 might be differentially cross-reactive. We cultured PBMCs from donor ML525 separately in the presence of the KF11 and [A2G,S4N]. After 12 days, we assessed the frequency of B*5703 KF11- and B*5703 [A2G,S4N]-specific T cell in individual cultures using tetramers. Interestingly, both cell lines grew at similar rates, and were highly cross-reactive as determined by double staining analysis using B*57^{KF11}- and B*57^{A2G,S4N}-specific tetramers (Fig. 3*A*). One hundred percent of [A2G,S4N]-specific T cell cross-reacted with B*57-KF11-specific T cells, but a small population of non-cross-reactive KF11-specific T lymphocytes were detected in both CTL

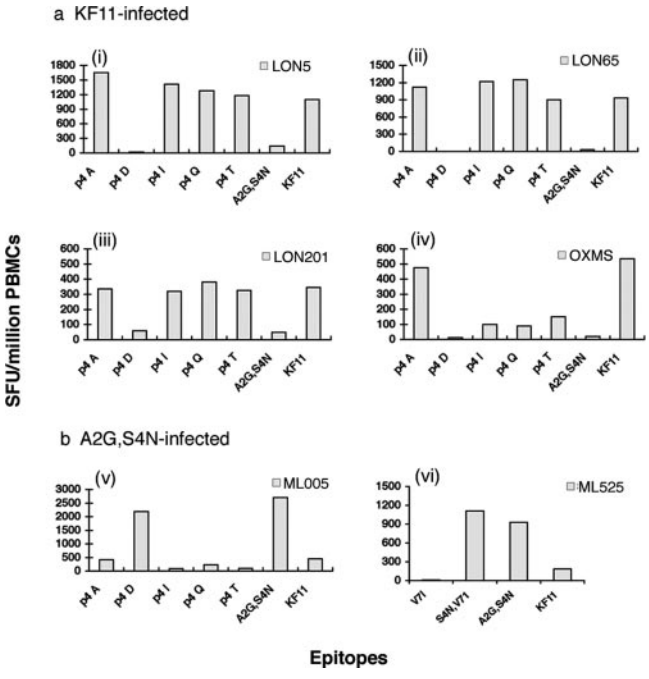

FIGURE 1. Differential recognition of p4 KF11 variants according to the predominant viral isolate. Cryopreserved PBMCs from B*57$^+$ patients harboring KF11 (*a*) and/or [A2G,S4N] (*b*) viruses were tested for their ability to recognize KF11 variants harboring a p4 amino acid mutation. Results are plotted as SFU per million PBMCs on the *y*-axis and p4 peptide variants are indicated along the *x*-axis.

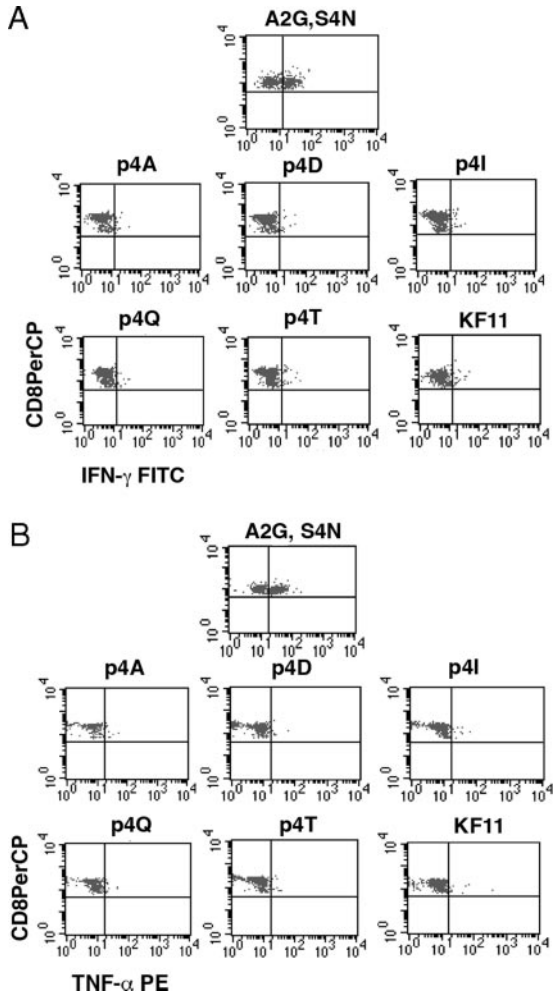

FIGURE 2. Cytokine production by [A2G,S4N]-specific CD8$^+$ T cell clones in response to p4 variants. [A2G,S4N]-specific T cell clones were tested for their ability to secrete IFN-γ (*A*) and TNF-α (*B*) in response to [A2G,S4N]-, KF11-, and KF11 p4 variant-pulsed BCL by intracellular cytokine staining. T cell clones were gated as a function of forward scatter (FSC) and side scatter (SSC) profiles. IFN-γ and TNF-α staining are indicated along the *x*-axis, and CD8 staining on the *y*-axis. Controls included BCLs incubated with T cells only. Peptide variants are denoted in bold.

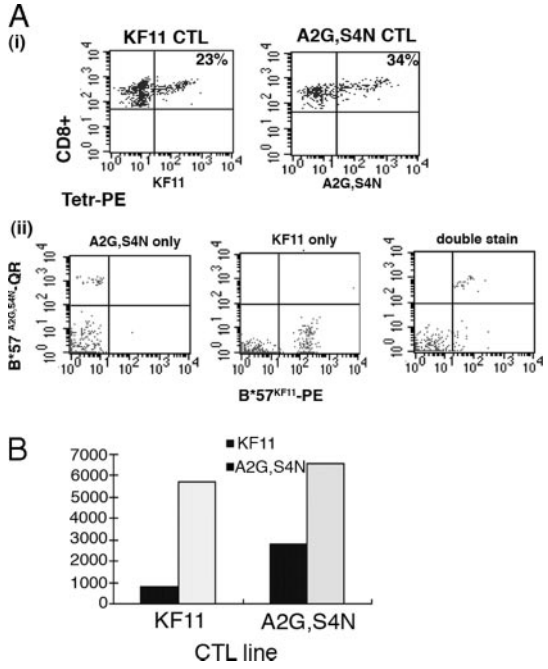

FIGURE 3. *A*, Proliferation of A2G,S4N-, and KF11-specific T cells from donor ML525. *i*, B*57 KF11 and A2G,S4N-specific tetramers were used to quantify the percentage of Ag-specific $CD8^+$ T lymphocytes in 12-day CTL lines cultured in the presence of the KF11 and A2G,S4N epitopes, respectively. Cells were gated as according to FSC and SSC profiles. Controls included CTLs incubated in the presence of anti-CD8 mAb only. CD8 expression is depicted on the *y*-axis and tetramer staining along the *x*-axis. *ii*, Dual staining tetramer analysis was performed to quantify the percentage of cross-reactive T cells in both A2G,S4N- (shown) and KF11- (not shown) specific CTL lines. Cells were gated as a function of FSC, SSC, and CD8 expression. B*57KF11 staining is indicated along the *x*-axis and B*57[A2G,S4N] along the *y*-axis. *B*, Preferential secretion of IFN-γ in response to [A2G,S4N] by KF11- and [A2G,S4N]-cultured CTL lines. Cryopreserved PBMCs from donor ML525 were cultured in the presence of KF11 and A2G,S4N peptides and, after 12 days, were tested for their ability to secrete IFN-γ in response to KF11 and A2G,S4N epitopes by ELISPOT analysis. Responses are reported as SFU per million CTLs.

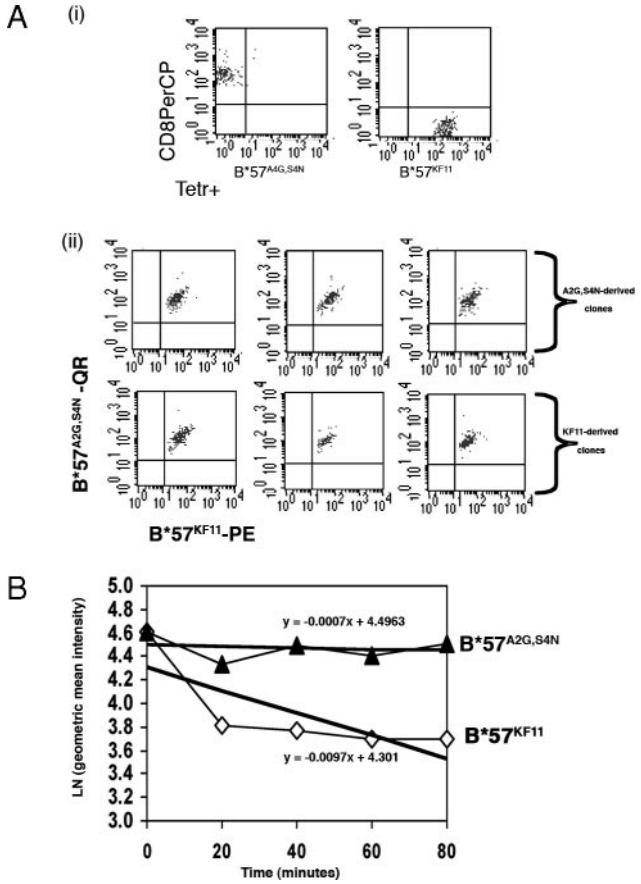

FIGURE 4. *A*, KF11- and [A2G,S4N]-grown T cell clones from donor ML525 display 100% cross-reactivity by dual tetramer staining analysis. *i*, $CD8^+$ T cell clones from donor ML525 were generated from [A2G,S4N]- and KF11-cultured CTL lines, and (*ii*) were triple stained with $B*57^{KF11}$-PE, $B*57^{A2G,S4N}$-QR tetramers, and anti-CD8 mAbs. T cells were gated as a function of FSS, SSC, and CD8 expression. Controls include T cell clones stained with anti-CD8 mAb plus $B*57^{KF11}$-PE or anti-CD8 mAb and $B*57^{A2G,S4N}$-QR tetramer only. $B*57^{KF11}$-PE staining is indicated along the *x*-axis, and $B*57^{A2G,S4N}$-QR tetramers staining on the *y*-axis. *B*, B*57-KF11 tetramers display more rapid dissociation kinetics from B*57-[A2G,S4N]-specific T cell clones than B*57-[A2G,S4N] tetramers. Tetramer decay analysis was performed to test whether $B*57^{KF11}$ and $B*57^{A2G,S4N}$ tetramers bound [A2G,S4N]-specific T cell clones with similar affinities. T cells were incubated separately with individual tetramers and delay was monitored at 20-min intervals over a total period of 80 min. Tetramer binding was analyzed by flow cytometry, and the natural log of the mean geometric intensity of FL-2 immunofluorescence for each samples (*y*-axis) were plotted against sampling time (*x*-axis).

lines. However, both KF11-and [A2G,S4N]-derived CTL lines preferentially secreted IFN-γ in response to [A2G,S4N], with limited recognition of KF11 (Fig. 3*b*). We also generated T cell clones from the individual CTL lines, and as demonstrated by tetramer staining, these were exclusively 100% cross-reactive irrespective of the epitope used to propagate them (Fig. 4*A*). Interestingly, however, tetramer decay analysis revealed that the $B*5703^{KF11}$ tetramer displayed weaker binding kinetics as compared with the $B*5703^{A2G,S4N}$ tetramer when tested on KF11-propaged clone p5-10 (Fig. 4*B*). We also assessed the ability of KF11- and [A2G,S4N]-derived clones to secrete IFN-γ, and to up-regulate the degranulation markers CD107a and b in response to KF11 and [A2G,S4N] epitopes. All KF11- and [A2G,S4N]-derived clones behaved identically in that [A2N,S4N] preferentially induced IFN-γ and CD107ab up-regulation with minimal recognition of KF11 (Fig. 5).

Structural determination of the KF11, [A2G,S4N], and [S4N,V7I] variant pMHC complexes

Our crystal structure of HLA-B*5703-KF11 shows that the unusual length of the 11-mer peptide is accommodated in the peptide-binding groove by the formation of a central peptide bulge. Peptide residues E6 and V7 are solvent exposed, project high above the peptide-binding groove, and are readily accessible for TCR recognition. The side chain of the p4 residue is also solvent exposed and on the basis of our cellular data, we predict that this is sufficient to be involved in TCR recognition. However, there may be a larger scale structural impact of p4 amino acid variation on the main chain bulge conformation. Therefore, to access whether any such conformational differences in the exposure of peptide residues could be responsible for the altered pattern of TCR recognition, we determined the structures of the [A2G,S4N] and [S4N,V7I] epitopes. Both structures were determined from crystals of the orthorhombic space group $P2_12_12_1$ which shared almost identical unit cell dimensions, with one HLA-B*5703-peptide complex per crystallographic asymmetric unit (Table III). The resolution of the x-ray diffraction data for the [A2G,S4N]- and [S4N,V7I]-B*5703 complexes (1.85 and 1.5 Å, respectively)

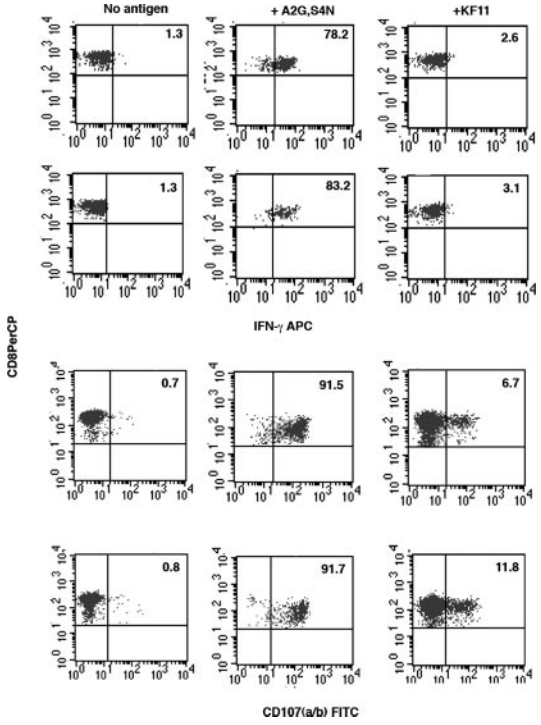

FIGURE 5. IFN-γ secretion and CD107ab expression in response to KF11 and A2G,S4N in KF11-cultured CD8$^+$ T cell clones, 5-10 and 5-4. CD8$^+$ T cell clones from donor ML525 were derived from KF11-cultured CTL lines and were tested for their ability to secrete IFN-γ and to express LAMP markers CD107a and b in response to KF11- and [A2G,S4N]-peptide-pulsed BCLs by ICS and flow cytometry analysis. T cells were gated as a function of FSC and SSC. IFN-γ secretion and CD107ab expression is indicated along the *x*-axis and CD8 staining on the *y*-axis.

allowed the atomic coordinates for the variant peptide residues (and associated bound water molecules) to be defined accurately permitting a detailed comparison with the KF11 peptide in HLA-B*5703 (12). Superimposition of the HLA-B*5703-KF11, -[A2G,S4N], and -[S4N,V7I] structures (based on their peptide-binding α 1/α 2 domain) reveals that the overall bulge conformation found in the main chain of the KF11 peptide is conserved with only minor adjustments in the conformations of some-solvent exposed side chains (Fig. 6). Although the A2G mutation is buried at

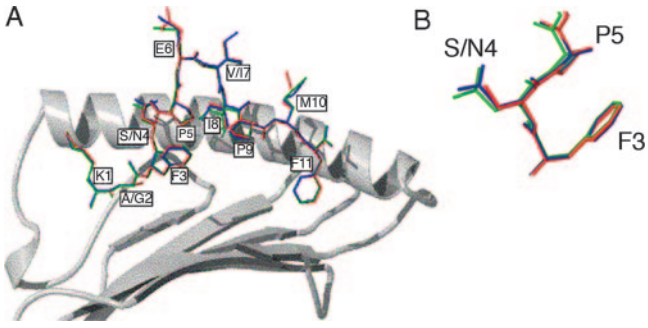

FIGURE 6. High resolution crystal structures of HLA-B*5703 in complex with KF11, A2G,S4N, and S4N,V7I illustrates the conserved orientation of the p4 S and N amino acids. *i*, A cross-sectional view of B*5703 in complex with KF11, A2G,S4N and S4N,V7I is shown (the B*5703 α2 helix has been removed for clarity). KF11 is illustrated in red, A2G,S4N in green, and S4N,V7I in blue. Orientation of the S and N side chains are similar relative to the peptide backbone. *ii*, An aerial view of peptide amino acids 3, 4, and 5 (from a TCR-docking perspective) highlighting minor p4S and P4 N positional alterations.

the B pocket, the S4N and V7I mutations are exposed within the region of the pMHC surface commonly observed to engage with TCRs (30) and thus may alter interactions with specific TCRs.

*TCR usage of B*57KF11-restricted CD8$^+$ T lymphocytes*

To elucidate the nature of the responding B*57-KF11 T cell repertoire, we evaluated the TCR selection in terms of the pattern of TCR V region usage and CDR3 sequence analysis. We focused on B*5701$^+$ and B*5703$^+$ patients infected with KF11- and [A2G,S4N] viruses. We used a combination of B*57-KF11/B*57-[A2G,S4N] tetramers and mAbs specific for TCR V region segments to determine TCR usage of B*KF11- and [A2G,S4N]-specific T cells, and this resulted in the identification of TCR V region usage for four of the patients studied. We also generated CTL lines, and cell clones specific for KF11/[A2G,S4N] from which the sequence of TCR Vα and Vβ gene segments were identified by PCR using a panel of predefined TCR Vα and Vβ primers. Using mAbs specific for TCR V region segments, we observed that three of the five B*5701$^+$ KF11-infected donors used a Vβ17 TCR. This receptor was expressed on 57–70% of PBMC-derived B*57-KF11-specific T lymphocytes in two donors (not assessed in OXAG). PCR analysis of T cell clones generated from these donors (LON005, OXAG, and LON201) used a Vβ17/Vα15 TCR pair (sequence nomenclature as defined by Arden et al. (31), which is equivalent to a TRBV19/TRAV5 TCR complex as defined by the international ImMunoGeneTics (IMGT) database (32)), and sequence analysis revealed almost complete conservation of the amino acid usage in both the Vα and Vβ CDR3 regions in all 3 donors, despite variation in nucleotide sequences (Fig. 7). The CDR3 Vα and Vβ regions were of average length and donors displayed conservation of glycine and tyrosine residues. B*5701$^+$ donor MS used a Vβ22 TCR (IMGT-TRBV2) and PCR analysis revealed this to comprise a Vβ22/Vα6 (IMGT-TRBV2/TRAV6) TCR pair; the Vβ22 CDR3 was short and the amino acids comprising the CDR3b loop were distinct from the conserved Vβ17 CDR3 sequence (data not shown). In B*5703$^+$ donor ML525 where [A2G,S4N] represented the dominant viral sequence, a Vβ15/Vα15 TCR (IMGT-TRBV24–1/TRAV5) combination was used, but the amino acid composition of this Vα15 CDR3 loop was highly distinct from the conserved Vα15/Vβ17 TCR (data not shown).

Discussion

HLA-B*5701 and -B*5703 are associated with slower HIV-1 disease progression. Both molecules present a similarly broad array of conserved epitopes to CD8$^+$ T cells, a feature that might contribute to their favorable association with prolonged AIDS-free survival.

Recently, escape mutations influencing the recognition of the dominant p24-derived epitopes IW9 and TW10 have been described (9, 33), and while both studies help define important correlates of B*57-mediated immunity it is likely that additional factors relate B*57 to prolonged survival. Previously, we focused on the B*57-KF11-specific CD8$^+$ T cell response which prevails during chronic HIV-1 infection. Here, we demonstrate that the HLA-B*57-KF11-specific immune response is consistently dominant during chronic disease in B*57$^+$ slow progressors. Formerly, we also demonstrated broad CD8$^+$ T cell-mediated recognition of diverse KF11 clade variants in B*57$^+$ slow progressors, and our recent crystallographic analysis of B*5703 in complex with the KF11 epitope (10, 12) provides an explanation for the inability of certain KF11 clade variants to induce CD8$^+$ T cell responses. However, differential recognition of the [A2G,S4N] and [S4N,V7I] clade variant harboring the same p4 mutation was less

A

Donor	V beta TCR	V/D (beta)	CDR 3	J (beta)	Valpha TCR	V(alpha)	CDR 3	J (alpha)
LON005	**VB17**	CAS	TGSYGYT	FG	**AV15.1**	CAL	SGGYQKVT	FG
OXAG	**VB17**	CAS	TGSYGYT	FG	**AV15.1**	CAV	SGGYQKVT	FG
LON201	**VB17**	CAS	TG[V]SYGYT	FG	**AV15.1**	CAG	SGGYQKVT	FG

B

(i)Vbeta 17 TcR

LON 005	C	A	S	**T**	G	-	**S**	**Y**	**G**	Y	T	F	G	**S**	**G**	T	R	**L**	**T**	V	T
	tgt	gcc	agt	**acc**	ggt	-	**tcc**	**tac**	**ggt**	tac	acc	ttc	ggt	**tcc**	**ggc**	acc	agg	**ctc**	**acg**	gtc	aca
OX AG	C	A	S	**T**	G	-	**S**	**Y**	**G**	Y	T	F	G	**S**	**G**	T	R	**L**	**T**	V	V
	tgt	gcc	agt	**aca**	ggg	-	**tcc**	**tat**	**ggt**	tac	acc	ttc	ggt	**tcg**	**ggg**	acc	agg	**tta**	**acc**	gtt	gta
LON 201	C	A	S	T	G	[V]	S	**Y**	G	Y	T	F	G	S	G	T	R	L	T	V	V
	tgt	gcc	agt	**acc**	ggg	**[gtc]**	**agc**	**tat**	**ggc**	tac	acc	ttc	ggt	**tcg**	**ggg**	acc	agg	**tta**	**acc**	gtt	gta

(ii)Valpha 15.1

LON 005	C	**A**	L	**S**	G	G	Y	Q	K	V	T	F	G	**T**	G	T	K	L	Q	V	I	P
	tgt	**gca**	**ctt**	**tca**	ggg	ggt	tac	cag	aaa	gtt	acc	ttt	gga	**act**	gga	aca	aag	ctc	caa	gtc	atc	cca
OX AG	C	**A**	V	**S**	G	G	Y	Q	K	V	T	F	G	V	G	T	K	L	Q	V	I	P
	tgt	**gcg**	**gtt**	**tct**	ggg	ggt	tac	cag	aaa	gtt	acc	ttt	gga	**gtt**	gga	aca	aag	ctc	caa	gtc	atc	cca
LON 201	C	**A**	G	**S**	G	G	Y	Q	K	V	T	F	G	**T**	G	T	K	L	Q	V	I	P
	tgt	**gca**	**ggg**	**tct**	ggg	ggt	tac	cag	aaa	gtt	acc	ttt	gga	**act**	gga	aca	aag	ctc	caa	gtc	atc	cca

FIGURE 7. TCR repertoire usage of B*57K11-specific T cell clones. TCR usage of K11- and A2G,S4N-specific T cell clones was determined by mRNA extraction, PCR, and sequencing analysis. *A*, TCR residues demarcating the boundary of the Vβ and Vα residues encompassing the CDR3 regions are underlined and include the conserved S at the end of the Vβ and Vα regions and conserved F residue of the Jβ and Jα regions, respectively. In LON201, a CDR3β valine insertion is denoted as [V]. *B*, Nucleotides encoding the conserved Vα15/Vβ17 TCR chains in B*57$^+$ donors are summarized. Silent nucleotide mutations encoding V region; CDR3 and J regions amino acids are highlighted in bold.

apparent; [A2G,S4N] represents important A/C clade variant viruses, and as such, warrants further investigation. We have now combined both structural and function analyses to define factors dictating the differential recognition of [A2G,S4N] and KF11. We specifically include B*5703$^+$ patients where the [A2G,S4N] virus represents a dominant infecting virus, as we previously observed preferential recognition of [A2G,S4N] and [S4N,V71] with minimal recognition of other KF11 clade variants in such donors (10) and our findings have recently been reiterated by others (34). Despite the small sample population, we observed distinct patterns of cross-reactivity, which varied according to the prevalent viral sequence B*5703$^+$ patients, where [A2G,S4N] represented the dominant viral species, displayed limited cross-reactivity, which was in sharp contrast to the broad pattern of p4 recognition in KF11-infected B*5701$^+$ individuals. These results were further exemplified in clones derived from [A2G,S4N]-infected patients; here, [A2G,S4N] induced preferential secretion of IFN-γ, TNF-α, and up-regulated the LAMP proteins CD107a and b. Collectively, these data imply that the subtle difference at p4 in the K11 epitope may lead to the selection of diverse TCR repertoires, with distinct cross-reactive potential.

B*5703$^+$ patient ML525 harbored both KF11 and [A2G,S4N] viruses, and attempts to grow T cell clones with distinct specificity for KF11 and [A2G,S4N] yielded unusual results. As assessed by tetramer staining all KF11- and [A2G,S4N]-derived T cell clones were 100% cross-reactive. Yet, despite this apparent cross-reactivity, all clones demonstrated functional specificity for the [A2G,S4N] epitope only, irrespective of the epitope used to propagate them. This disparity between tetramer staining analysis and functional studies is difficult to reconcile, however, the strong pattern of KF11-tetramer binding to [A2G,S4N]-specific T cells might result from increased pMHC-TCR avidity imposed by the artificially constructed tetrameric pMHC complex. These results reciprocate our previous findings where a B*5701^{A2G,S4N} tetramer reacted with 100% of PBMC-derived KF11-reactive T cells, yet [A2G,S4N] induced minimal IFN-γ secretion (10). Our preliminary tetramer-decay assay reveals that B*5703^{KF11} tetramers form less stable interactions with [A2G,S4N]-specific T cell clones when compared with B*5703^{A2G,S4N} tetramers. Hence, the interaction of KF11 tetrameric complexes with [A2G,S4N]-specific T cells ex vivo may represent an extended picture of the actual physiological interaction in vivo. Although N and S are both amino acids with polar side chains, they differ in size and hydrogen-bonding potential, which might alter the specificity of the p4-mediated interactions with TCRs in vivo.

In donor ML525, the KF11 epitope behaved like an altered peptide ligand and supported [A2G,S4N]-specific T cell division without inducing immune effector functions. In the context of chronic HIV-1 infection, this scenario might adversely influence the immune response: if, as in patient ML525, for example, KF11 represents the emerging virus, it is possible that in addition to priming KF11-specific T cells, this epitope would support the expansion of T cells specific for the index epitope, namely, [A2G,S4N]. As a result of prior activation, we would predict that [A2G,S4N]-specific memory T cell precursors are present at higher frequencies, and that KF11 priming might lead to the competitive outgrowth of [A2G,S4N]-reactive T cells with functional specificity for the [A2G,S4N] epitope only. Although we did observe the preferential expansion of donor ML525-derived [A2G,S4N]-specific T cell clones reflecting the prevalence of the [A2G,S4N] viral sequence,

we were unable to establish whether [A2G,S4N]-specific T cells were present at higher frequencies due to sample limitation. We are also unaware whether our patient was coinfected with both viral stains simultaneously, singularly on separate occasions, or developed either variant endogenously. Nonetheless, given our findings and as suggested by recent studies in mice (35), it may be crucial that clade variant epitopes, however similar, are incorporated into vaccines and administered simultaneously to ensure that distinct $CD8^+$ T populations are optimally primed. This approach may limit the biased expansion of T cells with restricted cross-reactive effector potential.

We performed a high-resolution structural analysis of B*5703 in complex with the [A2G,S4N] and [S4N,V7I] variant peptides to determine whether there was significant change in the structures of these epitopes compared with the B*5703-KF11 complex. Compared with KF11, the structures of the two variant peptides are broadly conserved by the formation of the bulged hairpin loop in the central portion of the peptide. The variant epitopes p4 and p7 remain solvent exposed within the standard TCR-binding footprint, making these side chains candidates for interaction with cognate TCRs. Given the large number of structural features, and in particular the extensive main chain surface area exposed by this pMHC complex, a given TCR may engage with multiple structural components; thus, the effects of the conservative alterations such as the S4N and V7I may not prevent TCR binding altogether. However, subtle differences in TCR-binding parameters have been shown to affect T cell activation/effector functions and variations in TCR-binding kinetics or thermodynamic parameters may result from minor alterations in peptide structure (36).

We also analyzed the nature of the TCR repertoire recognizing the highly unusual B*57KF11 complex and compared this to the TCR usage of B*57-[A2G,S4N]-specific T cells. Interestingly, three HLA-$B*5701^+$ donors infected with KF11 viruses, used a conserved Vα15 and Vβ17 TCR (or TRAV5/TRBV19 TCR (IMGT)), with striking conservation of CDR3 α and β amino acids, and interestingly, these T cells display greatest cross-reactivity ex vivo. Although Dong et al. (37) recently described the usage of the Vβ13.2 chain bearing a conserved CDR3 loop in response to a B*0801-restricted *nef* epitope, this is the first report of a bias in usage of both TCRα and β chains in human HIV-1 infection. The best-documented examples of conserved TCR $\alpha\beta$ chain usage have come from the study of influenza infection in humans, where the $CD8^+$ T cell responses to A*0201 complexed with the matrix peptide epitope, GILGFVFTL is dominated by a Vβ17/Vα10 TCR pair in most individuals (15). The Vβ17 CDR3 region is highly conserved and comprises an IRSSY motif (aa 97–101). The crystallographic structure of Vα10/Vβ17 in complex with A*0201-GILGFVFTL provides a structural explanation for the conserved TCR Vβ chain usage (38). In this TCR-pMHC complex residues D32 and Q52, unique to the Vβ 17 CDR1 and CDR2 loops, respectively, hydrogen bond the epitope and may define the specific orientation of the TCR onto the pMHC such that the conserved CDR3 β residue R98 inserts into a notch between the epitope and the HLA-A*0201 a2 helix. The R98 and S99 side chains create a dense hydrogen-bonding network between the TCR and pMHC. Similarly, $CD8^+$ T cell responses to the EBV EBNA3 epitope, FLRGRAYGL, are dominated by a common Vβ 6.1/Vα4.1 TCR (LC13) with conserved CDR3 α and β regions in $B*0801^+$ individuals (39) and recent crystallographic analysis of LC13 in complex with B*0801-FLRGRAYGL offers an explanation for the selection of the V and CDR3 α and β sequences comprising LC13 (40). Another striking example of TCRα, β, and CDR3 sequence conservation was recently documented in the study of TCR usage in SIV infection in macaques; here, the authors observed that the majority of macaques infected with SIVmac251 used conserved TCR Vβ chains when responding to the Mamu-A*01-restricted TL8 (Tat) and CM9 (gag) T cell epitopes and that many TL8- and CM9-specific TCR Vβ CDR3 regions were conserved at the amino acid level. Additionally, there was evidence for preferred TCR Vα chain usage in a small number of macaques responding to the TL8 epitope (41).

Given that the main chain conformation of the peptide epitope in B*5703-K11 is highly unusual it seems plausible that the available TCR repertoire may be limited in comparison to that capable of interacting with more conventional peptide-MHC complexes, hence the conserved pattern of TCR usage in $B*5701^+$ donors. However, B*5701 and B*5703 differ at amino acid positions (p) 114 and 116 which are situated near the F pocket; in B*5701, the p114 N and p116 S residues are replace by a D and Y in the B*5703 subtype, respectively. Based solely on our B*5703 crystallographic complexes, we predict that as p114 nor p116 side chains contribute few contact to peptide binding, KF11 and [A2G,S4N] should adopt similar conformations in B*5701 and B*5703. However, we cannot rule out the possibility that the overall orientation of KF11 or [A2G,S4N] in complex with B*5701 and B*5703 are dissimilar. For example, HLA-B2705 and 2709 differ only in residue 116 of the H chain (Asp in B*2705 and His in B(*)2709), yet display differential disease association with ankylosing spondylitis. Recently, Fiorillo et al. (42) demonstrated that the viral peptide, RRRWRRLTV (aa 236–244 of EBV, pLMP2), is presented by the B*2705 and B*2709 molecules in two drastically deviating conformations. In the absence of a B*5701-KF11 complex, we are unable to evaluate whether a similarly subtle difference between B*5701 and B*5703 profoundly impact upon the orientation of the KF11 clade variant epitope.

In summary, we have shown that although [A2G,S4N] and KF11 when in complex with B*5703 appear similar from a structural perspective, they behave differently in terms of the functional outcome they induce. In terms of TCR cross-reactivity, KF11 seems to support the outgrowth of $CD8^+$ T cells with a greater capacity for cross-reactivity in $B*5701^+$ donors, whereas in $B*5703^+$ patients the [A2G,S4N]-derived TCR repertoire are limited, particularly in terms amino acid recognition at p4. Interestingly, $B*5701^+$ patients infected with KF11 variants used a conserved TCR that cross-reacted with the majority of p4 variants; it is tempting to speculate that this receptor might select against the emergence of a p4 variant, although it displayed limited cross-reactivity to the most common database variant, [A2G,S4N]. Finally, whether our overall findings relate to the subtle p4 differences between KF11 and [A2G,S4N] or to the minor differences in the orientation of these peptide when presented by HLA-B*5701 and B*5703 that, in turn, dictate differential TCR repertoire selection are unknown. The TCR repertoire availability in different ethnic groups might also impact on TCR repertoire selection and TCR cross-reactivity. In-depth studies of larger $B*5701^+/B*5703^+$ cohorts, and if possible, $B*5701^+$ patients infected with [A2G,S4N], are necessary to evaluate these hypotheses.

Acknowledgments

We are grateful to the patients who participated in this study and to the clinical staff. We also thank the staff of the ESRF synchrotron facility for assistance with data collection.

Disclosures

The authors have no financial conflict of interest.

References

1. O'Brien, S. J., G. W. Nelson, C. A. Winkler, and M. W. Smith. 2000. Polygenic and multifactorial disease gene association in man: lessons from AIDS. *Annu. Rev. Genet.* 34: 563–591.
2. Kelleher, A. D., C. Long, E. C. Holmes, R. L. Allen, J. Wilson, C. Conlon, C. Workman, S. Shaunak, K. Olson, P. Goulder, et al. 2001. Clustered mutations in HIV-1 *gag* are consistently required for escape from HLA-B27-restricted cytotoxic T lymphocyte responses. *J. Exp. Med.* 193: 375–386.
3. Klein, M. R., I. P. Keet, J. D'amaro, R. J. Bende, A. Hekman, B. Mesman, M. Koot, L. P. De Waal, R. A. Coutinho, and F. Miedema. 1994. Associations between HLA frequencies and pathogenic features of human immunodeficiency virus type 1 infection in seroconverters from the Amsterdam cohort of homosexual men. *J. Infect. Dis.* 169: 1244–1249.
4. Costello, C., J. Tang, C. Rivers, E. Karita, J. Meizen-Derr, S. Allen, and R. A. Kaslow. 1999. HLA-B*5703 independently associated with slower HIV-1 disease progression in Rwandan women. *AIDS* 13: 1990–1991.
5. Migueles, S. A., M. S. Sabbaghian, W. L. Shupert, M. P. Bettinotti, F. M. Marincola, L. Martino, C. W. Hallahan, S. M. Selig, D. Schwartz, J. Sullivan, and M. Connors. 2000. HLA B*5701 is highly associated with restriction of virus replication in a subgroup of HIV-infected long term nonprogressors. *Proc. Natl. Acad. Sci. USA* 97: 2709–2714.
6. Tang, J., S. Tang, E. Lobashevsky, A. D. Myracle, U. Fideli, G. Aldrovandi, S. Allen, R. Musonda, and R. A. Kaslow. 2002. Favorable and unfavorable HLA class I alleles and haplotypes in Zambians predominantly infected with clade C human immunodeficiency virus type 1. *J. Virol.* 76: 8276–8284.
7. Goulder, P. J., M. Bunce, P. Krausa, K. Mcintyre, S. Crowley, B. Morgan, A. Edwards, P. Giangrande, R. E. Phillips, and A. J. Mcmichael. 1996. Novel, cross-restricted, conserved, and immunodominant cytotoxic T lymphocyte epitopes in slow progressors in HIV type 1 infection. *AIDS Res. Hum. Retroviruses* 12: 1691–1698.
8. Migueles, S. A., A. C. Laborico, H. Imamichi, W. L. Shupert, C. Royce, M. Mclaughlin, L. Ehler, J. Metcalf, S. Liu, C. W. Hallahan, and M. Connors. 2003. The differential ability of HLA B*5701$^+$ long-term nonprogressors and progressors to restrict human immunodeficiency virus replication is not caused by loss of recognition of autologous viral *gag* sequences. *J. Virol.* 77: 6889–6898.
9. Leslie, A. J., K. J. Pfafferott, P. Chetty, R. Draenert, M. M. Addo, M. Feeney, Y. Tang, E. C. Holmes, T. Allen, J. G. Prado, et al. 2004. HIV evolution: CTL escape mutation and reversion after transmission. *Nat. Med.* 10: 282–289.
10. Gillespie, G. M., R. Kaul, T. Dong, H. B. Yang, T. Rostron, J. J. Bwayo, P. Kiama, T. Peto, F. A. Plummer, A. J. McMichael, and S. L. Rowland-Jones. 2002. Cross-reactive cytotoxic T lymphocytes against a HIV-1 p24 epitope in slow progressors with B*57. *AIDS* 16: 961–972.
11. Ferrari, G., J. R. Currier, M. E. Harris, S. Finkelstein, A. De Oliveira, D. Barkhan, J. H. Cox, M. Zeira, K. J. Weinhold, N. Reinsmoen, et al. 2004. HLA-A and -B allele expression and ability to develop anti-Gag cross-clade responses in subtype C HIV-1-infected Ethiopians. *Hum. Immunol.* 65: 648–659.
12. Stewart-Jones, G. B., G. Gillespie, I. M. Overton, R. Kaul, P. Roche, A. J. McMichael, S. Rowland-Jones, and E. Y. Jones. 2005. Structures of three HIV-1 HLA-B*5703-peptide complexes and identification of related HLAs potentially associated with long-term nonprogression. *J. Immunol.* 175: 2459–2468.
13. Altfeld, M., M. M. Addo, E. S. Rosenberg, F. M. Hecht, P. K. Lee, M. Vogel, X. G. Yu, R. Draenert, M. N. Johnston, D. Strick, et al. 2003. Influence of HLA-B57 on clinical presentation and viral control during acute HIV-1 infection. *AIDS* 17: 2581–2591.
14. Gillespie, G. M., M. R. Wills, V. Appay, C. O'Callaghan, M. Murphy, N. Smith, P. Sissons, S. Rowland-Jones, J. I. Bell, and P. A. Moss. 2000. Functional heterogeneity and high frequencies of cytomegalovirus-specific CD8$^+$ T lymphocytes in healthy seropositive donors. *J. Virol.* 74: 8140–8150.
15. Lehner, P. J., E. C. Wang, P. A. Moss, S. Williams, K. Platt, S. M. Friedman, J. I. Bell, and L. K. Borysiewicz. 1995. Human HLA-A0201-restricted cytotoxic T lymphocyte recognition of influenza A is dominated by T cells bearing the Vβ17 gene segment. *J. Exp. Med.* 181: 79–91.
16. Kaul, R., F. A. Plummer, J. Kimani, T. Dong, P. Kiama, T. Rostron, E. Njagi, K. S. Macdonald, J. J. Bwayo, A. J. McMichael, and S. L. Rowland-Jones. 2000. HIV-1-specific mucosal CD8$^+$ lymphocyte responses in the cervix of HIV-1-resistant prostitutes in Nairobi. *J. Immunol.* 164: 1602–1611.
17. Appay, V., D. F. Nixon, S. M. Donahoe, G. M. Gillespie, T. Dong, A. King, G. S. Ogg, H. M. Spiegel, C. Conlon, C. A. Spina, et al. 2000. HIV-specific CD8$^+$ T cells produce antiviral cytokines but are impaired in cytolytic function. *J. Exp. Med.* 192: 63–75.
18. Betts, M. R., J. M. Brenchley, D. A. Price, S. C. De Rosa, D. C. Douek, M. Roederer, and R. A. Koup. 2003. Sensitive and viable identification of antigen-specific CD8$^+$ T cells by a flow cytometric assay for degranulation. *J. Immunol. Methods* 281: 65–78.
19. Jansen, C. A., S. Kostense, K. Vandenberghe, N. M. Nanlohy, I. M. De Cuyper, E. Piriou, E. H. Manting, F. Miedema, and D. Van Baarle. 2005. High responsiveness of HLA-B57-restricted Gag-specific CD8$^+$ T cells in vitro may contribute to the protective effect of HLA-B57 IN HIV-infection. *Eur. J. Immunol.* 35: 150–158.
20. Wilson, J. D., G. S. Ogg, R. L. Allen, P. J. Goulder, A. Kelleher, A. K. Sewell, C. A. O'Callaghan, S. L. Rowland-Jones, M. F. Callan, and A. J. McMichael. 1998. Oligoclonal expansions of CD8$^+$ T cells in chronic HIV infection are antigen specific. *J. Exp. Med.* 188: 785–790.
21. Weekes, M. P., M. R. Wills, K. Mynard, A. J. Carmichael, and J. G. Sissons. 1999. The memory cytotoxic T-lymphocyte (CTL) response to human cytomegalovirus infection contains individual peptide-specific CTL clones that have undergone extensive expansion in vivo. *J. Virol.* 73: 2099–2108.
22. Kissinger, C. R., D. K. Gehlhaar, and D. B. Fogel. 1999. Rapid automated molecular replacement by evolutionary search. *Acta Crystallogr. D Biol. Crystallogr.* 55: 484–491.
23. Brunger, A. T., P. D. Adams, G. M. Clore, W. L. Delano, P. Gros, R. W. Grosse-Kunstleve, J. S. Jiang, J. Kuszewski, M. Nilges, N. S. Pannu, and E. Al. 1998. Crystallography & NMR system: a new software suite for macromolecular structure determination. *Acta Crystallogr. D. Biol. Crystallogr.* 54: 905–921.
24. Jones, T. A., J. Y. Zou, S. W. Cowan, and Kjeldgaard. 1991. Improved methods for building protein models in electron density maps and the location of errors in these mode. *Acta Crystallogr. A* 47: 110–119.
25. Stuart, D. I., M. Levine, H. Muirhead, and D. K. Stammers. 1979. Crystal structure of cat muscle pyruvate kinase at a resolution of 2.6 A. *J. Mol. Biol.* 134: 109–142.
26. Morris, R. J., A. Perrakis., and E. Al. 2002. ARP/wARP's model-building algorithms. I. The main chain. *Acta Crystallogr. D Biol. Crystallogr.* 58: 968–975.
27. Murshudov, G. N. 1997. Refinement of macromolecular structures by the maximum-likelihood method. *Acta Crystallogr. D Biol. Crystallogr.* 53: 240–245.
28. Hubbard, S. J. T., J. M. 1996. "NACCESS" computer program version 2.1.1. University College London, London.
29. Esnouf, R. M. 1999. Further additions to MolScript version 1.4, including reading and contouring of electron-density maps. *Acta Crystallogr.* 55: 938–940.
30. Rudolph, M. G., and I. A. Wilson. 2002. The specificity of TCR/pMHC interaction. *Curr. Opin. Immunol.* 14: 52–65.
31. Arden, B., S. P. Clark, D. Kabelitz, and T. W. Mak. 1995. Human T-cell receptor variable gene segment families. *Immunogenetics* 42: 455–500.
32. Lefranc, M. P., C. Pommie, M. Ruiz, V. Guidicelli, E. Foulquier, L. Truong, V. Thouvenin-Contet, and G. Lefranc. 2003. IMGT unique numbering for immunoglobulin and T cell receptor variable domains and Ig superfamily V-like domains. *Dev. Comp. Immunol.* 27: 55–77.
33. Draenert, R., S. Le Gall, K. J. Pfafferott, A. J. Leslie, P. Chetty, C. Brander, E. C. Holmes, S. C. Chang, M. E. Feeney, M. M. Addo, et al. 2004. Immune selection for altered antigen processing leads to cytotoxic T lymphocyte escape in chronic HIV-1 infection. *J. Exp. Med.* 199: 905–915.
34. Currier, J. R., M. E. Harris, J. H. Cox, F. E. McCutchan, D. L. Birx, S. Maayan, and G. Ferrari. 2005. Immunodominance and cross-reactivity of B*5703 restricted CD8 T lymphocytes from HIV type 1 subtype C-infected Ethiopians. *AIDS Res. Hum. Retroviruses* 21: 239–245.
35. Singh, R. A., J. R. Rodgers, and M. A. Barry. 2002. The role of T cell antagonism and original antigenic sin in genetic immunization. *J. Immunol.* 169: 6779–6786.
36. Krogsgaard, M., and M. M. Davis. 2005. How T cells "see" antigen. *Nat. Immunol.* 6: 239–245.
37. Dong, T., G. Stewart-Jones, N. Chen, P. Easterbrook, X. Xu, L. Papagno, V. Appay, M. Weekes, C. Conlon, C. Spina, et al. 2004. HIV-specific cytotoxic T cells from long-term survivors select a unique T cell receptor. *J. Exp. Med.* 200: 1547–1557.
38. Stewart-Jones, G. B., A. J. Mcmichael, J. I. Bell, D. I. Stuart, and E. Y. Jones. 2003. A structural basis for immunodominant human T cell receptor recognition. *Nat. Immunol.* 4: 657–663.
39. Argaet, V. P., C. W. Schmidt, S. R. Burrows, S. L. Silins, M. G. Kurilla, D. L. Doolan, A. Suhrbier, D. J. Moss, E. Kieff, T. B. Suclley, et al. 1994. Dominant selection of an invariant T cell antigen receptor in response to persistent infection by Epstein-Barr virus. *J. Exp. Med.* 180: 2335–2340.
40. Kjer-Nielsen, L., C. S. Clements, A. W. Purcell, A. G. Brooks, J. C. Whisstock, S. R. Burrows, J. McCluskey, and J. Rossjohn. 2003. A structural basis for the selection of dominant $\alpha\beta$ T cell receptors in antiviral immunity. *Immunity* 18: 53–64.
41. Price, D. A., S. M. West, M. R. Betts, L. E. Ruff, J. M. Brenchley, D. R. Ambrozak, Y. Edghill-Smith, M. J. Kuroda, D. Bodgan, K. Kunstman, et al. 2004. T cell receptor recognition motifs govern immune escape in acute SIV infection. *Immunity* 21: 793–803.
42. Fiorillo, M. T., C. Ruckert, M. Hulsmeyer, R. Sorrentino, W. Saenger, A. Ziegler, and B. Uchanska-Ziegler. 2005. Allele-dependent similarity between viral and self-peptide presentation by HLA-B27 subtypes. *J. Biol. Chem.* 280: 2962–2971.